J. Biochem. **141,** 363–376 (2007)
doi:10.1093/jb/mvm041

Functional and Structural Characterization of D-Aspartate Oxidase from Porcine Kidney: Non-Michaelis Kinetics due to Substrate Activation

Atsushi Yamamoto*, Hiroyuki Tanaka, Tetsuo Ishida and Kihachiro Horiike

Department of Biochemistry and Molecular Biology, Shiga University of Medical Science, Seta, Ohtsu, Shiga 520-2192, Japan

Received December 25, 2006; accepted January 9, 2007; published online January 18, 2007

D-Aspartate oxidase (DDO, EC 1.4.3.1) catalyzes dehydrogenation of D-aspartate to iminoaspartate and the subsequent re-oxidation of reduced FAD with O_2 to produce hydrogen peroxide. In the mammalian neuroendocrine system, D-aspartate, a natural substrate, plays important roles in the regulation of the synthesis and secretion of hormones. To elucidate the kinetic and structural properties of native DDO, we purified DDO from porcine kidney to homogeneity, cloned the cDNA, and over-expressed the enzyme in *Escherichia coli*. The purified DDO was a homotetramer with tightly-bound FAD. The enzyme consisted of 341 amino acids and had GAGVMG as the dinucleotide binding motif and a C-terminal SKL peroxisomal-targeting signal sequence. Porcine DDO showed a strong affinity for *meso*-tartrate ($K_d = 118\,\mu M$). The oxidase exhibited pronounced substrate activation at D-aspartate and D-glutamate concentrations, [S], higher than 0.2 and 4 mM, respectively, and the [S]/*v* versus [S] plot showed marked downward curvature (*v*, the initial velocity), whereas substrate inhibition occurred with *N*-methyl-D-aspartate. These kinetic properties of DDO suggested that at high substrate concentrations, the FAD-reduced form of the enzyme also catalyzes the reaction: the oxidative half-reaction precedes the reductive one. The present direct approach to the analysis of non-Michaelis kinetics is indispensable for understanding the functional properties of DDO.

Key words: D-aspartate oxidase, D-aspartate, cDNA cloning, neuroendocrine system, porcine kidney.

Abbreviations: DDO, D-aspartate oxidase; NMDA, *N*-methyl-D-aspartic acid; MBTH, 3-methyl-2-benzothiazolinone hydrazone hydrochloride; RACE, rapid amplification of cDNA ends.

D-Aspartate exists abundantly in mammalian pineal, pituitary, and adrenal glands (*1–7*), which are members of the neuroendocrine system. Recent studies indicate that D-aspartate is involved in the synthesis of hormones and their secretion in the neuroendocrine system (*2*, *5*, *8–13*). Importantly, the localization of D-aspartate in the system is inversely correlated to that of D-aspartate oxidase (DDO; EC 1.4.3.1), an FAD-dependent peroxisomal enzyme (*2*). DDO is the only enzyme known to be responsible for metabolizing D-aspartate. DDO catalyzes the oxidative deamination of dicarboxylic D-amino acids using O_2 to yield the corresponding imino acids and hydrogen peroxide; the imino acids are rapidly hydrolyzed to 2-oxo acids and ammonia. DDO-deficient mice show elevated levels of D-aspartate in the pituitary intermediate lobe, leading to diminished synthesis of proopiomelanocortin, and then melanotropin-dependent influences decrease to elevate body mass (*13–15*). To further elucidate the roles of both D-aspartate and DDO in the neuroendocrine system, it is important to examine the biochemical properties of DDO.

Difficulty in the purification of DDO from mammalian tissues has hampered the biochemical characterization of this oxidase. Purification of DDO from bovine kidney has succeeded (*16*), whereas DDO has been only partially purified from porcine kidney (*17*) and thyroid glands (*18*). On the other hand, the recombinant mammalian DDO has been obtained for human (*19*), bovine (*20*, *21*), and mouse (*22*). Among these mammalian DDOs, the most detailed kinetic analysis has been carried out for bovine DDO (*23–25*). Bovine DDO exhibits significant substrate activation at D-aspartate concentrations above 1.0 mM (*24*, *25*): its Lineweaver-Burk plot shows an apparent downward curvature (*25*). As the physiological concentrations of D-aspartate are in the range of 0–3 mM (*1*, *3*, *5*), it is important to elucidate the mechanism of this substrate activation. However, prior to this study, all the apparent k_{cat} and K_m values reported for DDO have been determined using only data obtained at a limited range of substrate concentrations where a Michaelian behavior is apparently observed.

To explain the non-Michaelian kinetics of DDO described above, Hamilton has proposed a reaction mechanism where not only the oxidized form of DDO (E_o) but also the reduced form of DDO (E_r) accepts substrate and catalyzes the reaction (see Fig. 1) (*25*).

*To whom correspondence should be addressed. Tel: +81 77 548 2158, Fax: +81 77 548 2157,
E-mail: atsu@belle.shiga-med.ac.jp

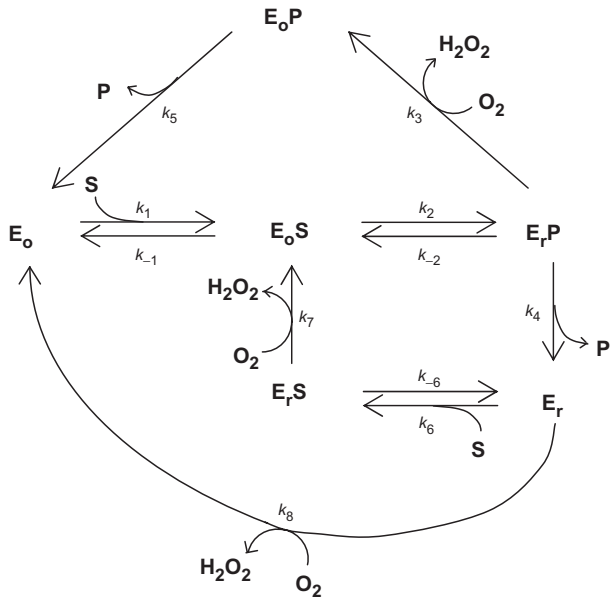

Fig. 1. **A mechanism for D-aspartate oxidase reaction.** E_o is the enzyme with bound FAD oxidized. E_r is the enzyme with bound FAD fully reduced. S is a D-amino acid substrate. P is the α-imino acid product, which is rapidly and non-enzymatically hydrolyzed to the corresponding 2-oxo acid and ammonia after the release from the enzyme. E_oS and E_rS are the complex of oxidized and reduced enzyme with substrate, respectively. E_oP and E_rP are the complex of oxidized and reduced enzyme with product, respectively. Rate constants for relevant elementary reactions are shown in the figure.

This model has never been applied to systematically analyze the actual kinetic data of DDO.

In the present study, for the first time, we purified DDO from porcine kidney, cloned the cDNA for the DDO, and expressed the enzyme in *Escherichia coli*. Both the native and recombinant porcine DDOs showed significant substrate activation at higher concentrations of D-aspartate and D-glutamate. We have proposed a reaction mechanism which combines the Hamilton model for DDO (*25*) and the reaction mechanism proposed for D-amino acid oxidase (*26*, *27* and the references cited therein). On the basis of our model, the steady-state kinetic properties of DDO were successfully described with four kinetic parameters. This study indicates that under physiological concentrations of D-amino acid substrate and O_2, both the oxidized and reduced forms of DDO catalyze the reaction with different catalytic competence.

EXPERIMENTAL PROCEDURES

Materials—Porcine kidney from female *Sus scrofa* was purchased from a local slaughter house and kept at about −35°C until use. D-Aspartic acid, D-glutamic acid, *N*-methyl-D-aspartic acid (NMDA), sodium pyruvate, 2-oxoglutaric acid, 2,4-dinitrophenylhydrazine, FAD, sodium potassium L-tartrate, L-tartaric acid, D-tartaric acid, *meso*-tartaric acid, and malonic acid were all purchased from Wako Pure Chemical Industries (Osaka, Japan). 3-Methyl-2-benzothiazolinone hydrazone hydrochloride (MBTH) was obtained from Aldrich and catalase was from Boehringer-Mannheim. All other chemicals were of analytical grade.

Enzyme Assays—During the purification, the 2,4-dinitrophenylhydrazine method of Yamada *et al*. (*28*) was used to measure oxalacetate generation from D-aspartate. The standard assay mixture (0.1 ml) contained 50 mM sodium pyrophosphate, pH 8.3, 50 mM D-aspartate, 50 μM FAD, and 10 μg catalase. The reaction was initiated by adding enzyme solutions. One unit of DDO activity was defined as the amount of enzyme producing 1 μmol of oxalacetate per min at 37°C under the standard assay conditions.

Kinetic data was obtained in a wide concentration range of D-amino acid by two methods. In the first method, polarographic measurement using a Model 5331 O_2 electrode (Yellow Springs, OH, USA) was used to measure O_2 consumption. We used a glass reaction vessel maintained at 37°C and put the reaction vessel in a box that was easy to purge with argon, as described previously (*29*). The reaction mixture (1.78 ml) contained 50 mM sodium pyrophosphate, pH 8.3, 50 μM FAD, 180 μg catalase, and varying amounts of D-amino acid substrate and O_2. The O_2 concentration was varied over the range of 1–1,000 μM using the method described previously (*29*). The reaction was started by the addition of an enzyme solution. The second method was the HPLC assay developed recently by us (*30*). This method quantified the accumulation of oxalacetate during incubation at 37°C for 0–30 min. Reactions were carried out in 200 μl of 50 mM sodium pyrophosphate, pH 8.3, containing 50 μM FAD, 20 μg catalase, and varying amounts of D-amino acid substrate. The reaction was started by the addition of the enzyme (1 μl) and stopped by the addition of 12.5% trichloroacetic acid (40 μl).

The enzyme stock solution for kinetics was prepared by overnight dialysis of 200 μl of the purified DDO stored at −20°C against 2 liters of 50 mM potassium phosphate, pH 6.75, containing 1 μM FAD and 10 mM Na,K L-tartrate. The concentration of the holo-subunit of the DDO stock solution was determined spectrophotometrically using a Shimadzu UV-2550 spectrometer and assuming a molar absorption coefficient of 11.3 $mM^{-1} cm^{-1}$ at 455 nm (*31*).

The effects of pH on the activity of native and recombinant DDO for D-aspartate were examined at 37°C and at the ionic strength of 0.3 M (adjusted with NaCl) using the following buffer solutions: 0.1 M Mes-NaOH (pH 5.5–6.5), 0.1 M HEPES-NaOH (pH 6.5–7.5), 0.1 M Tris-HCl (7.5–8.5), and 0.1 M CHES-NaOH (8.5–9.5). The reaction mixture contained 50 mM D-aspartate in air-saturated buffers. The oxalacetate generation was measured using the 2,4-dinitrophenylhydrazine method, as described above.

Purification of Native DDO—Unless otherwise stated, all procedures were conducted at about 4°C and all buffers contained 10 mM Na,K L-tartrate. HPLC was performed at room temperature. The buffers used for the homogenization of porcine kidney contained no Na,K L-tartrate. We purified DDO from 90 g of porcine kidney cortex. Extremely gentle homogenization of the cortex was essential to avoid the contamination of certain

proteins that were difficult to remove by later chromatographic steps. Thus, we treated 10 g of the kidney cortex at one time by the following method, and repeated the same procedure 9 times. We diced the cortex and homogenized partially in a glass homogenizer with only three gentle strokes of the piston using 10 ml of 5 mM MOPS, pH 7.4, containing 250 mM sucrose, 1 mM EDTA, and 0.1% (v/v) ethanol. The partial homogenates were centrifuged at $200 \times g$ for 5 min. The supernatant obtained was centrifuged at $5{,}500 \times g$ for 10 min. The precipitates were then completely homogenized with 10 mL of 20 mM potassium phosphate, pH 5.4, containing 10 μM FAD and 0.3 mM EDTA using the glass homogenizer. The obtained homogenates were combined (crude extract). The pH of the crude extract was adjusted to 5.4 at 4°C using 1.67 M acetic acid. The crude extract was then incubated at 55°C for 15 min using a water bath. After cooling down to 10°C, the heat-treated extract was centrifuged at $10{,}000 \times g$ for 10 min. The supernatant (heat-treatment) was applied to an SP-Toyopearl column (5 × 2 cm, Tosoh) preequilibrated with 20 mM potassium phosphate, pH 5.4, containing 10 μM FAD and 0.3 mM EDTA. The column was washed with 5 volumes of the equilibration buffer, and the enzyme was then eluted with 20 mM potassium phosphate, pH 8.4, containing 10 μM FAD and 0.3 mM EDTA. The active fractions were pooled (SP-Toyopearl) and loaded onto a Q-Sepharose column (2.5 × 5 cm, Pharmacia) preequilibrated with the buffer used above for the elution. The column was developed with the buffer and the active fractions in the flow-through were pooled (Q-Sepharose). The Q-Sepharose fraction was diluted 2-fold with 2 M potassium phosphate, pH 6.75, containing 10 μM FAD, and 0.3 mM EDTA. The diluted Q-Sepharose fraction was applied to a PPG-Toyopearl column (2.5 × 2 cm, Tosoh) preequilibrated with 1 M potassium phosphate, pH 6.75, containing 10 μM FAD, and 0.3 mM EDTA. The column was washed with five volumes of the buffer and then the enzyme was eluted with 200 mM potassium phosphate, pH 6.75, containing 10 μM FAD, 0.3 mM EDTA, and 200 mM KCl. The pooled active fractions (PPG-Toyopearl) were concentrated to about 0.2 ml using an Ultra PL-30 membrane filter (Amicon) and a Microcon YM-30 membrane filter (Amicon) in that order. An aliquot (20 μl) of the concentrate was repeatedly injected into a TSKgel SuperSW3000 column (4.6 × 300 mm, Tosoh) preequilibrated with 200 mM potassium phosphate, pH 6.75, containing 10 μM FAD, 0.3 mM EDTA, and 200 mM KCl. Elution was performed with the buffer at a flow rate of 0.2 ml/min. The active fractions (SuperSW3000) were pooled and concentrated to about 0.2 ml with an Amicon Ultra PL-30 membrane filter. The concentrated SuperSW3000 fraction was dialyzed against 1 liter of 1 mM potassium phosphate, pH 6.75, containing, 0.3 mM EDTA overnight. The dialyzed sample was applied to a hydroxyapatite column (1 × 1.5 cm, Nacalai tesque) preequilibrated with 1 mM potassium phosphate, pH 6.75, containing 10 μM FAD, 1 mM Na,K L-tartrate, and 0.3 mM EDTA. The column was washed with five volumes of the equilibration buffer and then the enzyme was eluted with 20 mM potassium phosphate, pH 5.4, containing 10 μM FAD and 0.3 mM EDTA. The pooled active fractions (hydroxyapatite) were applied to a Bioassist-5S column (4.6 × 50 mm, Tosoh) preequilibrated with 20 mM potassium phosphate, pH 5.4, containing 10 μM FAD and 0.3 mM EDTA. The column was developed with a linear gradient of KCl concentration (16.7 mM/min) in the equilibration buffer at a flow rate of 0.5 ml/min. Each of the active fractions was subjected to SDS-PAGE, and the fractions showing a single protein band were pooled. The pooled fraction (Bio-5S) was stored at −20°C. No loss of activity was observed after at least one month storage.

Protein content was determined using a BCA protein assay kit (Wako Pure Chemical Industries) with bovine serum albumin as a standard.

Cloning of Porcine DDO cDNA—Total RNA was extracted from porcine kidney cortex using an RNeasy Midi kit (Qiagen). First strand cDNA was prepared from the total RNA using Super Script III First Strand Synthesis System (Invitrogen). The cDNA strand of porcine DDO was amplified by PCR using the first strand cDNA as a template and the following two sets of primers: forward primers, 5′-CCCATGGATACAGTACGGATTG-3′ and 5′-GCTTTTTCAGAGACAGGCCCATG-3′; reverse primers, 5′-GAGCTTAACGCCCTATGTCATAGC-3′ and 5′-GCTAATTTCTGCATCTGGGGAC-3′. These primers were designed on the basis of the nucleotide sequence of bovine kidney DDO (*20*). PCR was performed using Platinum *pfx* DNA polymerase kit (Invitrogen) using the following conditions: 94°C for 15 s, 55°C for 30 s, and 68°C for 1 min, for 35 cycles. The main PCR product obtained was cloned into pCR4-TOPO vector (Invitrogen) and sequenced using an ABI Prism 310 DNA Sequencer (Applied Biosystems) with a DYEnamic ET terminator kit (Amersham). The nucleotide sequence of the PCR product was similar to the corresponding sequences of bovine and human DDOs. To obtain the complete cDNA by rapid amplification of cDNA ends (RACE), we designed primers specific to porcine DDO on the basis of this nucleotide sequence. RACE was performed using a Gene Racer kit (Invitrogen) and the following primer sets: for the primary PCR, Gene Racer 5′ Primer and 5′-TTCTGGGGCCATCTGCTGTTGT-3′ for 5′-RACE, Gene Racer 3′ Primer and 5′-CCCATGGATACAGTACG GATTG-3′ for 3′-RACE; for the secondary nested PCR, Gene Racer 5′ nested Primer and 5′-CTACAGCTTTGAT TTAGGAGCAGGGG-3′ for nested 5′-RACE, Gene Racer 3′ nested Primer and 5′-ACTTTGAGCACTTGGCCCC TCA-3′ for nested 3′-RACE. The nucleotide sequences of the PCR products were determined as described above.

Expression of Recombinant Porcine DDO—The open reading frame for porcine DDO cDNA was amplified by PCR using the first strand cDNA and the following primers, 5′-**CACC**ATGGATACAGTACGGATTG-3′ and 5′-CTACAGCTTTGATTTAGGAGCAGGG-3′ (the sequence of the forward primer indicated in bold was added for directional TOPO cloning). The PCR product was cloned into pET100/D-TOPO vector (Invitrogen). The obtained expression plasmid (pETDDO) was used to transform BL 21 Star (DE 3) *E. coli* cells (Invitrogen). The cells were grown at 37°C to a turbidity of 0.5–0.8 at 600 nm in LB medium containing 100 μg/ml ampicillin. After the

addition of isopropyl-1-thio-β-D-galactopyranoside to a final concentration of 1 mM, the culture was grown for a further 4–6 h to induce the expression of His_6-tagged DDO. The cells were harvested by centrifugation, and stored at −20°C until use.

Purification of Recombinant DDO—The *E. coli* cells (10 g) were resuspended in 90 ml of 20 mM sodium phosphate, pH 7.4, containing 10 μM FAD and 10 mM Na,K L-tartrate. The cells were disrupted on ice by sonication while maintaining the temperature below 10°C. The homogenates were centrifuged at $8,000 \times g$ for 10 min. Solid ammonium sulfate was added to the supernatant to 30% saturation. After incubation for 30 min with continuous stirring, the solution was centrifuged at $10,000 \times g$ for 10 min. Solid ammonium sulfate was further added to the resultant supernatant to 50% saturation and the mixture was incubated for 30 min, and then the precipitate was collected by centrifugation. The precipitate was dissolved in 3.0 ml of 20 mM sodium phosphate, pH 7.4, containing 10 μM FAD, 10 mM Na,K L-tartrate, 0.5 M NaCl, and 20 mM imidazole, and dialyzed against 3 liters of the phosphate buffer for 4 h. After removing insoluble materials by centrifugation, the dialysate was applied to a His Trap HP column (1 ml bed volume, Amersham) preequilibrated with the same buffer as used for the dialysis. The column was washed with five volumes of the buffer and then the recombinant enzyme was eluted with 20 mM sodium phosphate, pH 7.4, containing 10 μM FAD, 10 mM Na,K L-tartrate, 0.5 M NaCl, and 0.5 M imidazole. The pooled active fractions were concentrated to about 2.0 ml using an Ultra PL-30 membrane filter and a Microcon YM-30 membrane filter in that order. An aliquot of the concentrate (200 μl) was applied to a TSKgel $G3000SW_{XL}$ column (7.8×300 mm) preequilibrated with 200 mM potassium phosphate, pH 6.75, containing 10 μM FAD and 0.3 mM EDTA. Elution was performed with the phosphate buffer at a flow rate of 0.8 ml/min and the active fractions were collected. To remove the N-terminal His_6-tag, the pooled active fractions were digested with 10 U of enterokinase using an EK Max kit (Invitrogen) for 24 h at 37°C. The recombinant DDO was recovered from the digests by gel filtration on a TSKgel SuperSW3000 column (4.6×300 mm) using the same phosphate buffer at a flow rate of 0.2 ml/min.

SDS-Polyacrylamide Gel Electrophoresis—SDS-PAGE was performed as described by Laemmli (*32*) using a 12.5% gel. Proteins in the gel were stained using a silver staining kit (Wako Pure Chemical Industries). N-Terminal sequencing was performed on polyvinylidene difluoride electrotransferred samples using an automated protein sequencer (Model 477A, Applied Biosysytem).

Molecular Weight Determination—The molecular weight of native DDO was determined by low-angle laser light scattering measurement combined with gel chromatography as described previously (*33*) using a TSKgel SuperSW3000 column (4.6×300 mm). The molecular weight standards used were ovalbumin monomer ($M_r = 45{,}000$), bovine albumin monomer ($M_r = 66{,}300$) and catechol 2,3-dioxygenase (*Pseudomonas putida*, homotetramer of $M_r = 140{,}624$); the former two proteins were from Sigma and the third was purified by the reported method (*34*). The subunit molecular weight of DDO was determined by matrix-assisted laser desorption mass spectrometry using a Voyager-DE RP mass spectrometer (PerSeptive Biosystems) and α-cyano-4-hydroxycinnamic acid as a matrix-forming material. Catechol 2,3-dioxygenase (*Pseudomonas putida*, subunit molecular weight of 35,156) was used for mass calibration.

Thin-layer Chromatography—To remove the exogenous FAD added in the buffer used for purification, an aliquot of the purified DDO (50 μg) was passed through a Sephadex G-25 column (5×30 mm) equilibrated with 50 mM potassium phosphate, pH 6.75. The enzyme eluted at the void volume was incubated at 80°C for 20 min in the dark, and then centrifuged to pellet the denatured protein. An aliquot of the supernatant was analyzed by thin-layer chromatography on a Linear-K Preadsorbent TLC Plate (Whatman, USA) with 5% $Na_2HPO_4 \cdot 12H_2O$ as the eluent. As a control, authentic FAD, FMN, and riboflavin were run separately or as a mixture under the same conditions.

Titration of DDO with Dicarboxylic Acids—The recombinant DDO (10 μM, 1.0 ml) was titrated at 37°C with *meso*-tartrate, L-tartrate, D-tartrate, and malonate, respectively, in 50 mM potassium phosphate, pH 6.75, by step-wise addition of 1 M aqueous dicarboxylic acid solution. The recombinant DDO stock solution was prepared by overnight dialysis of the purified enzyme against 50 mM potassium phosphate, pH 6.75 containing 1 μM FAD. After the end of the titration, we measured the pH of the sample; the change in pH due to titration was maximally 0.2. The change in FAD absorption induced by the addition of the dicarboxylic acids was measured using a Shimadzu UV-2550 spectrometer. The difference between absorption at 480 nm and 700 nm as a function of the total concentration of the dicarboxylic acid was analyzed by the following equation using a non-linear least-squares method.

$$\Delta A = \frac{2\Delta A_\infty L_t}{\left(E_t + K_d + L_t + \sqrt{(E_t + K_d - L_t)^2 + 4K_d L_t}\right)} \quad (1)$$

where ΔA_∞ is the maximal absorbance difference, E_t is the total concentration of the holo-subunit of DDO, L_t the total concentration of dicarboxylic acid, and K_d the dissociation constant.

Analysis of Kinetic Data—Porcine DDO showed non-hyperbolic kinetics for D-aspartate and D-glutamate. We analyzed the kinetic data on the basis of the reaction mechanism shown in Fig. 1. By applying steady-state approximation to this reaction model, we can obtain the initial velocity (v) as a function of the D-amino acid substrate concentration [S] as follows:

$$\frac{v}{E_t} = \frac{a_1[S] + a_2[S]^2}{a_3 + a_4[S] + a_5[S]^2} \quad (2)$$

where E_t is the total concentration of the holo-subunit of DDO, and a_i ($i = 1$–5) is the function of the O_2 concentration and the rate constants for the elementary reactions given in Fig. 1 (a_i is given by Eqs E2–E6 in

Appendix). Equation 2 can be expressed in the following form after some algebra.

$$\frac{[S]}{(v/E_t)} = \frac{A_3 + A_4[S] + A_5[S]^2}{A_1 + [S]} \quad (3)$$

where A_i is defined by a_i/a_2 ($i = 1$, 3, 4, and 5), respectively. The relation between these parameters and the elementary rate constants are given by Eqs E8–E11 in the Appendix and listed in Table 3. We analyzed the initial velocity (v) data on the basis of Eq. 3 using the [S]/v versus [S] plot (Hanes-Woolf plot) and non-linear least-squares method.

The initial velocity as a function of the O_2 concentration is a 3/3 rational function, more complex than Eq. 2. However, under the reaction conditions saturated with the D-amino acid substrate, this 3/3 rational function approximates to the following 2/2 rational function, which is similar to Eq. 3.

$$\frac{[O_2]}{(v/E_t)} = \frac{B_3 + B_4[O_2] + B_5[O_2]^2}{B_1 + [O_2]} \quad (4)$$

where B_i ($i = 1$, 3–5) is given by the Eqs E24–E27 in the Appendix, respectively. When the concentration of O_2 is much smaller than B_1 and B_4/B_5, then Eq. 4 approximates to the following linear function (see Appendix):

$$\frac{[O_2]}{(v/E_t)} = \frac{K_{mO2}^{app}}{k_{cat}^{app}} + \frac{1}{k_{cat}^{app}}[O_2] \quad (5)$$

The initial velocity data as a function of the O_2 concentration using saturating levels of D-amino acid substrate (25–50 mM) obeyed apparently to a simple hyperbolic function. Therefore, the dependence of the initial velocity on the O_2 concentration was analyzed based on Eq. 5.

RESULTS

Purification of Porcine DDO—The DDO purified from porcine kidney migrated as a single band with molecular weight of 38,000 during SDS-PAGE (Fig. 2A), indicating that the purified enzyme was homogeneous. The results of a typical purification procedure are shown in Table 1. The purified DDO had a specific activity of 62 μmol/min/mg protein. Only a single peak of DDO activity appeared for all chromatographic steps performed.

The subunit molecular weight was estimated to be 37,000 by mass spectrometry (Fig. 2B). The molecular weight of native enzyme was determined to be of 146,000 by low-angle laser light scattering photometry (Fig. 2C), predicting a homotetrameric structure for native DDO. Determination of the N-terminal amino acid sequence of the purified enzyme failed probably due to the modification of the N-terminal residue.

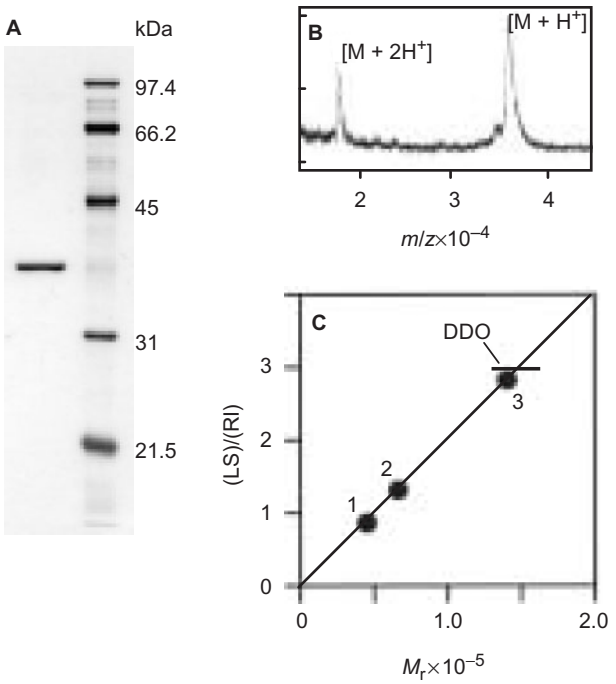

Fig. 2. **Molecular size of porcine kidney DDO.** (**A**) SDS-PAGE analysis under reducing conditions. The purified enzyme (0.5 μg) was loaded onto a 12.5% polyacrylamide gel (the left lane). (**B**) Mass spectrum of the purified enzyme. Desalted enzyme preparation was mixed with α-cyano-4-hydroxycinnamic acid and applied to a time-of-flight mass spectrometer. (**C**) Low-angle laser light scattering measurement combined with gel chromatography. The purified native enzyme (20 μg) was applied to a TSKgel SuperSW3000 column (4.6 × 300 mm) and the elution was detected by a low-angle laser light scattering photometer and a differential refractometer in that order. The ratio of the output of the light scattering photometer (LS) to that of the refractometer (RI) was plotted against molecular weight: 1, ovalbumin monomer ($M_r = 45{,}000$); 2, bovine albumin monomer ($M_r = 66{,}300$); 3, catechol 2,3-dioxygenase ($M_r = 140{,}624$).

Table 1. **Purification of D-aspartate oxidase from 90 g of porcine kidney cortex.**

Purification step	Total volume (ml)	Protein content (mg)	Total activity (units)	Specific activity (units/mg)	Yield (%)	Purification (fold)
Crude extract	200	1200	92	0.08	100	1
Heat treatment	190	230	60	0.26	65	3.3
SP-Toyopearl	150	40	44	1.1	48	14
Q-Sepharose	150	22	33	1.5	36	19
PPG-Toyopearl	23	3.2	23	7.2	25	90
SuperSW3000	4	0.81	12	15	13	188
Hydroxyapatite	6	0.62	11	18	12	225
Bio-5S, 1st.	1	0.16	7	44	7.6	550
Bio-5S, 2nd.	0.6	0.09	5.6	62	6.1	775

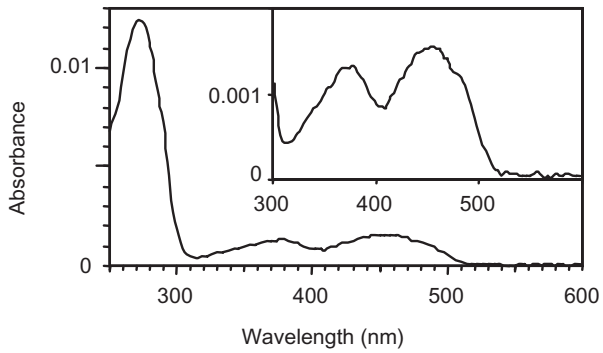

Fig. 3. **Absorption spectrum of porcine DDO.** The inset is an enlargement of the spectrum in the visible wavelength region. The purified native enzyme (1 μg) was applied to a TSKgel G2000SW$_{XL}$ column (2.0 × 50 mm) preequilibrated with 50 mM potassium phosphate, pH 6.75, containing 5 μM FAD. The column was developed with the same buffer at a flow rate of 0.1 ml/min. The elution was monitored using a photodiode array detector (Shimadzu SPD-M10A$_{VP}$). The absorption spectrum of the elution buffer was subtracted from that at the peak of the enzyme elution.

The absorption spectrum of the purified DDO (Fig. 3) showed maxima at 273, 374, and 452 nm and a shoulder around 480 nm (A_{273}/A_{455} ratio of 7.9). Unlike the DDO from bovine kidney (*16*), the purified enzyme showed no absorption above 600 nm, indicating that the enzyme did not contain 6-hydroxy-FAD. The yellow chromophore contained in the enzyme was completely released from the protein moiety by heat-denaturation. The isolated chromophore migrated as a single spot on the thin-layer chromatograph with the same R_f value of 0.83 as FAD migrated; R_f values for FMN and riboflavin were 0.64, and 0.54, respectively (data not shown). These results strongly suggest that the purified enzyme contains noncovalently bound FAD as the sole coenzyme. The recombinant enzyme (see later section) also contained only FAD as judged by the absorption spectrum and the thin-layer chromatographic analysis.

Cloning and Sequencing of the DDO Gene—The nucleotide sequence of porcine DDO cDNA and the deduced amino acid sequence are shown in Fig. 4. The cDNA contains 1984 base-pairs coding for a 341-amino-acid protein with a molecular weight of 37,315. This is in agreement with the molecular weight estimated by SDS-PAGE and mass spectrometry (Fig. 2). The cDNA exhibits a 5′ untranslated region of 73 base-pairs and a 3′ untranslated region of 885 base-pairs. A polyadenylation signal (AATAAA) is located 21 base-pairs upstream from the beginning of the poly A tail.

Porcine DDO consisted of exactly the same number of amino acids (341) as other mammalian DDOs, and the identity in amino-acid sequence between porcine DDO and other mammalian DDOs was 88%, 83%, and 75% for bovine, human, and mouse DDOs, respectively (Fig. 5). The GAGVMG sequence in the N-terminal sequence of porcine DDO (indicated by solid underline in Fig. 4) has a feature identical to the dinucleotide binding motif of GXGXXG, suggesting that these residues are responsible for FAD binding. The C-terminal SKL sequence (indicated by broken underline in Fig. 4) is identical to one of the minimal peroxisome-targeting signals (*35*), indicating that porcine DDO is a peroxisomal enzyme. As indicated in Fig. 5, the three arginine residues (R216, R237, and R278) and one tyrosine residue (Y223) are conserved; these are proposed as catalytically important residues (*19*, *22*, *36*).

Overexpression of Recombinant Porcine DDO—Recombinant DDO expressed in *E. coli* cells carrying pETDDO was purified by a four-step procedure as described under "EXPERIMENTAL PROCEDURES". About 1 mg of homogeneous DDO was obtained from 3 liters of isopropyl-1-thio-β-D-galactopyranoside-induced culture. The recombinant DDO had a specific activity of 58 μmol/min/mg protein, and showed a single protein band corresponding to a molecular weight of 38,000 on an SDS-PAGE gel (data not shown). Unlike the native DDO, the N-terminal amino acid sequence of the recombinant DDO could be determined to be identical to that predicted from the nucleotide sequence up to residue 41 (data not shown).

Comparison between Recombinant and Native DDO Activities—Both native and recombinant DDO showed similar specific activities of 62 and 58 μmol/min/mg protein under standard assay conditions. First, we compared the pH-dependence of the initial velocity between the native and recombinant DDO using 50 mM D-aspartate and air-saturated buffers (Fig. 6A). Both enzymes showed an essentially identical pH-profile of their activity: the activity increased gradually as pH increased from pH 5.5 to 7.5, exhibited an almost constant value over pH 7.5 to 9.0, and decreased as the pH increased over pH 9.0. At pH 8.3, the activity (40–45 μmol/min/mg protein, Fig. 6A) was less than the specific activities determined under standard assay conditions (60 μmol/min/mg protein). This difference is probably due to the effect of the buffer species pyrophosphate or Tris on the enzyme, as observed for D-amino acid oxidase. Next, we examined at pH 8.3 the dependence of the initial velocity on the concentration of D-aspartate. No significant difference was found in the dependence of the reaction catalyzed by the native and recombinant DDO on the concentration of D-aspartate (Fig. 6B). Therefore, in the following, we used the recombinant enzyme for the study of the steady-state kinetics.

Kinetic Properties of Porcine DDO—First, we obtained initial velocity of DDO over a wide concentration range of D-aspartate (0.01–80 mM) using air-saturated buffer (pH 8.3) (Fig. 7A–D). As is apparent in Fig. 7C and D, the [S]/*v* versus [S] plot curved downward over the concentration range of 0.1 to 1 mM, indicating that substrate activation occurred as the D-aspartate concentration increased above 0.2 mM. Second, we examined the dependence of the activity on the concentration of D-glutamate (0.01–100 mM) (Fig. 7E–H). The [S]/*v* versus [S] plot curved downward over the concentration range of 2 to 40 mM (Fig. 7G and H), although the curvature was less prominent than that observed for D-aspartate. Significant substrate activation occurred at concentrations of D-glutamate above 4 mM. Lastly, we obtained the initial velocity as a function of the concentration of NMDA (0.01–100 mM) (Fig. 7I–L). In this case,

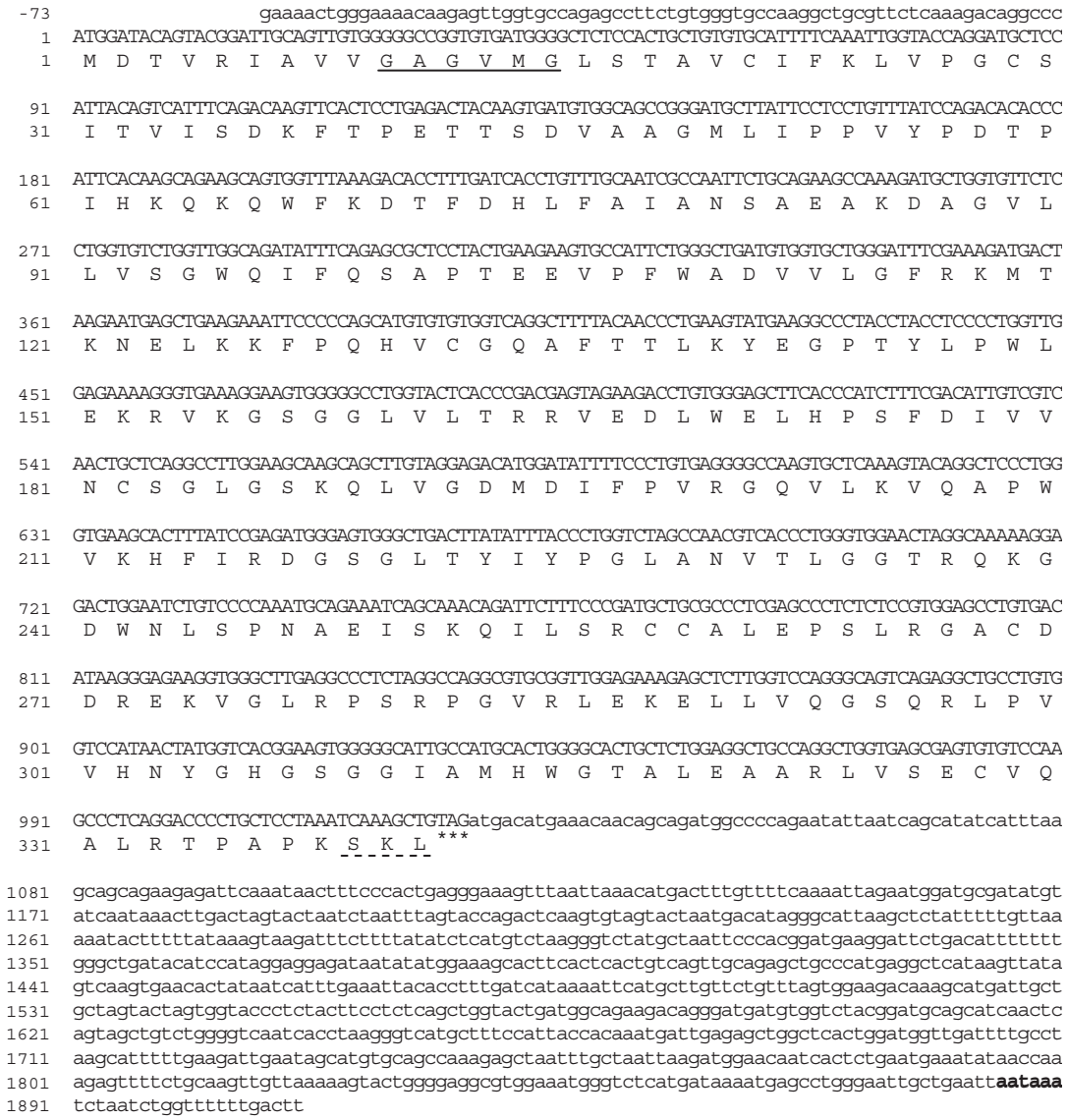

Fig. 4. **Nucleotide and deduced amino acid sequences of the porcine DDO cDNA.** ∗, the termination TAG codon. —, the amino acid sequence specific for a FAD-binding motif of GXGXXG. ---, the C-terminal SKL sequence is known as a peroxisomal targeting signal. Bold letters, a polyadenylation sequence in the 3′-untranslated region.

the [S]/*v* versus [S] plot was almost linear (Fig.7K and L), and the initial velocity showed a weak tendency to decrease as the NMDA concentration increased over 20 mM (Fig. 7I). This result suggested that a weak but significant level of substrate inhibition occurred when the NMDA concentration was higher than 20 mM.

All of the kinetic data shown in Fig. 7 fitted to Eq. 3 with good quality; the best fit curves are drawn in Fig. 7. The best-fit parameters are summarized in Table 2. Relationships between the elementary rate constants in Fig. 1 and the kinetic parameters of A_1, A_3, A_4, and A_5 are listed in Table 3. As explained in the Appendix, the initial part of the [S]/*v* versus [S] plot is approximately linear and the slope of this linear portion is A_4/A_1. At higher values of [S], the plot becomes approximately linear again, but the slope of the liner portion is A_5. Using the parameter values listed in Table 2, the value of the initial slope (A_4/A_1) was calculated to be 0.380 and 0.313 s for D-aspartate and D-glutamate, respectively, about 14- and 3-fold larger than the corresponding value of the slope at higher [S] (A_5), whereas the A_4/A_1 value (0.0215 s) was slightly smaller than the A_5 value of for NMDA. Hence, these calculations confirm the downward curvature of the [S]/*v* versus [S] plot (substrate activation) for D-aspartate and D-glutamate, and the upward curvature of the plot (substrate inhibition) for NMDA.

Figure 8 shows the dependence of the initial velocity of DDO on a range of the O_2 concentration (10–10,00 μM) in the presence of 25 mM D-aspartate, 50 mM D-glutamate, or 25 mM NMDA. We could not determine the initial velocity at the O_2 concentration above 1 mM due to the low solubility of O_2. All of the data obtained apparently

```
                                                                      60
Porcine: MDTVRIAVVGAGVMGLSTAVCIFKLVPGCSITVISDKFTPETTSDVAAGMLIPPVYPDTP
Bovine : ************************S*M****************************T*****
Human  : ***A*********V********S*L**R**V*I*******D***********HT*****
Mouse  : ****C********I*****A**SQ*****TV*****R***D***N********HT*A***
                                                                     120
Porcine: IHKQKQWFKDTFDHLFAIANSAEAKDAGVLLVSGWQIFQSAPTEEVPFWADVVLGFRKMT
Bovine : *Q*******E********V*********************I******************
Human  : **T*****R***N**********G****H*********T******************
Mouse  : VPT**RC*RE**E**SE**K****A****H********R*V*A****************
                                                                     180
Porcine: KNELKKFPQHVCGQAFTTLKYEGPTYLPWLEKRVKGSGGLVLTRRVEDLWELHPSFDIVV
Bovine : *D*********F*H******C***A*****Q*****N***I****I**************
Human  : EA*******Y*F********C*C*A********I*****WT****I**************
Mouse  : EA***R***Y*F********C*TSA******R*I******L****I******Q*******
                                                                     240
Porcine: NCSGLGSKQLVGDMDIFPVRGQVLKVQAPWVKHFIRDGSGLTYIYPGLANVTLGGTRQKG
Bovine : *******R**A**SK*********************S**********VS**********
Human  : *******R**A**SK*********Q******E**************TSH**********
Mouse  : *******RR***DPM*S*******QAR**********G****V***MSY**********
                                                                     300
Porcine: DWNLSPNAEISKQILSRCCALEPSLRGACDIREKVGLRPSRPGVRLEKELLVQGSQRLPV
Bovine : ******D*****E*L************Y*L********T**S********A*D*R*****
Human  : ******D**N*RE**********H***N*********Y******QT***ARDG******
Mouse  : ***R**D**L*RE*F****T*****HRAY**K***************Q*****R*Q*T***
                                                                    341
Porcine: VHNYGHGSGGIAMHWGTALEAARLVSECVQALRTPAPKSKL
Bovine : **HY*****************T***NE***V**********
Human  : **H********SV***T***********H*****I***N*
Mouse  : ***********SV***S****T***M**IHT*****SL***
```

Fig. 5. **Comparison among the primary structures of mammalian DDOs.** Asterisks indicate that corresponding amino acid residues are identical in all these proteins. The numbering system of the upper line refers to the porcine DDO sequence. The amino acid residues in boxes indicate the active site residues of DDO proposed by Sacchi *et al*. (*36*). The accession numbers of the primary structures of porcine, bovine, human, and mouse DDO are AB271762, X95310, D89858, and AK085947, respectively.

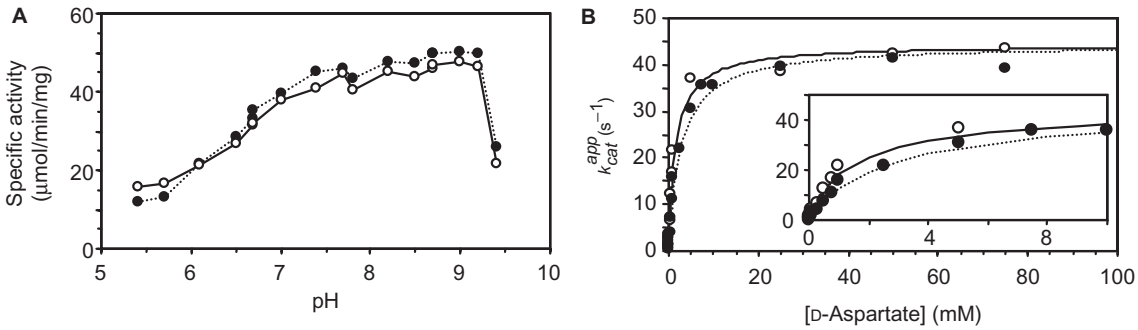

Fig. 6. **Comparison between kinetic properties of native and recombinant DDOs.** (**A**) pH-dependence of the specific activities of native (•) and recombinant (○) DDO at 37°C. The reaction mixtures (100 μl) contained 50 mM D-aspartate and the following buffers: 0.1 M Mes-NaOH (pH 5.5–6.5), 0.1 M HEPES-NaOH (pH 6.5–7.5), 0.1 M Tris-HCl (7.5–8.5), and 0.1 M CHES-NaOH (8.5–9.5). The ionic strength of all buffers was 0.3 M (adjusted with NaCl). (B) Initial velocities of native (•) and recombinant (○) DDO at 37°C as a function of the concentration of D-aspartate. The inset shows an enlargement of the data in the concentration range from 0 to 10 mM. The buffer used was 50 mM sodium pyrophosphate, pH 8.3.

obeyed the ordinary Michaelis–Menten equation. Therefore, we fitted the data to Eq. 5 as described in "EXPERIMENTAL PROCEDURES". The best-fit values of apparent k_{cat} and K_{mO2} are listed in Table 4, and the theoretical curves are drawn in Fig. 8 using these values. The apparent k_{cat}/K_{mO2} value of porcine DDO for D-aspartate and NMDA was 2.81×10^5 and $3.16 \times 10^5\,M^{-1}s^{-1}$, respectively, and that for D-glutamate was $5.48 \times 10^4\,M^{-1}s^{-1}$, about one-order smaller compared to the two former D-amino-acids.

Titration of DDO by Dicarboxylic Acids—To purify native and recombinant DDOs with higher levels of specific activity, the addition of Na,K L-tartaric acid to the buffer used was indispensable. We examined the interaction of DDO with malonate and three stereoisomers of tartrate by measuring the change induced in the visible absorption of DDO upon the addition of these dicarboxylates. Figure 9 shows typical titration data for L-tartrate. The visible spectrum of the L-tartrate-DDO complex (Fig. 9A) showed a considerable increase of the

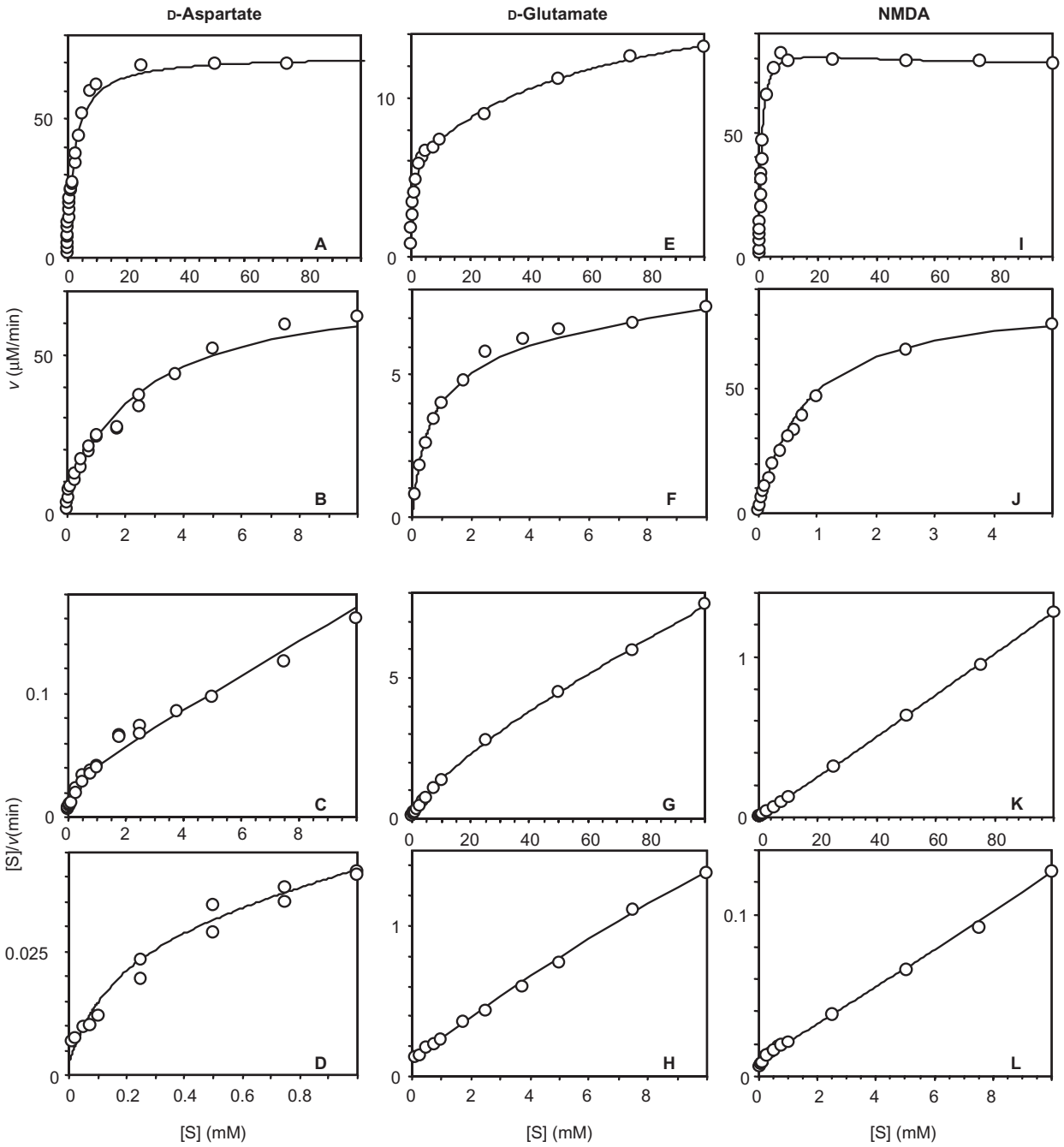

Fig. 7. **Initial velocity of porcine DDO as a function of the concentration of D-amino acid substrates.** The steady-state reactions were performed at 37°C using air-saturated 50 mM sodium pyrophosphate, pH 8.3 ($[O_2] = 240–260\ \mu M$). The final concentration of the holo-subunit of the enzyme was 32.2 nM. The lines drawn in the figures are made on the basis of Eq. 3 using the corresponding best-fit values of the four kinetic parameters listed in Table 2. Figures **A**, **E**, and **I** are the v versus [S] plot for D-aspartate, D-glutamate, and NMDA, respectively. Figures **B**, **F**, and **J** are an enlargement of the corresponding v versus [S] plot in the lower substrate concentration region. Figures **C**, **G**, and **K** are the [S]/v versus [S] plot for D-aspartate, D-glutamate, and NMDA, respectively. Figures **D**, **H**, and **L** are an enlargement of the corresponding [S]/v versus [S] plot in the lower substrate concentration region.

shoulder around 480 nm and a red shift of the absorption maximum from 452 to 456 nm. All of the data obtained fitted well to Eq. 1 (see the theoretical curve drawn in Fig. 9B). The K_d values are shown in Table 5. Among the three stereo-isomers of tartrate, DDO showed the highest affinity to *meso*-tartrate (K_d value of 118 μM).

DISCUSSION

In spite of the physiological importance of DDO especially in the mammalian neuroendocrine system, biochemical characterization of DDO has been very limited compared to D-amino acid oxidase, which

Table 2. **Kinetic parameters of porcine DDO for dicarboxylic D-amino acids.** The kinetic parameters for DDO were determined at 37°C with air-saturated 50 mM sodium pyrophosphate (pH 8.3) ($[O_2] = 240–260\,\mu M$). The data was fitted to Equation 3 and the best-fit values for the parameters are listed with the standard deviation.

Substrate	A_1 (mM)	A_3 ($M^2 \cdot s$)	A_4 ($M \cdot s$)	A_5 (s)
D-Aspartate	0.177 ± 0.549	$(8.94 \pm 104) \times 10^{-10}$	$(6.72 \pm 3.66) \times 10^{-5}$	$(2.66 \pm 0.08) \times 10^{-2}$
D-Glutamate	22.8 ± 2.7	$(4.12 \pm 2.14) \times 10^{-6}$	$(7.14 \pm 0.78) \times 10^{-3}$	0.107 ± 0.007
NMDA	24.3 ± 0.91	$(4.59 \pm 1.60) \times 10^{-7}$	$(5.22 \pm 0.38) \times 10^{-4}$	$(2.53 \pm 0.04) \times 10^{-2}$

Table 3. **Relation between kinetic parameters and elementary rate constants.** The elementary rate constants are shown in Fig. 1. The derivation of these relations is given in the Appendix. Equilibrium constant of K_R, K_O, and K_2 is defined as follows: $K_R = k_{-6}/k_6$, $K_O = k_{-1}/k_1$, and $K_2 = k_{-2}/k_2$.

Parameter	Expression	Unit
A_1	$k_8[O_2]\left(\frac{1}{k_6} + K_R \cdot \frac{1}{k_7[O_2]}\right)$	M
A_3	$A_1\left[\frac{1}{k_1} + K_O \cdot \frac{1}{k_2} + K_O \frac{1}{(k_3[O_2] + k_4)}\right]$	$M^2 \cdot s$
A_4	$\left(\frac{1}{k_3[O_2] + k_4}\right)\left[\begin{array}{l} K_O\left(K_2 + \frac{k_4}{k_2} + \frac{k_3[O_2]}{k_2}\right) + \frac{k_3[O_2]}{k_1} \\ \quad + A_1\left(1 + K_2 + \frac{k_4}{k_2} + \frac{k_3[O_2]}{k_2} + \frac{k_3[O_2]}{k_5} + \frac{k_4}{k_8[O_2]}\right) \end{array}\right]$	$M \cdot s$
A_5	$\left(\frac{1}{k_3[O_2] + k_4}\right)\left(1 + K_2 + \frac{k_4}{k_2} + \frac{k_3[O_2]}{k_2} + \frac{k_3[O_2]}{k_5} + \frac{k_4}{k_7[O_2]}\right)$	s

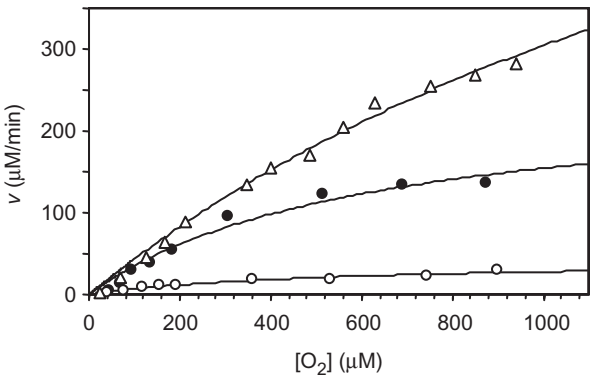

Fig. 8. **Initial velocity of porcine DDO as a function of the O_2 concentration.** The steady-state reactions were performed at 37°C using 50 mM sodium pyrophosphate, pH 8.3, containing 25 mM D-aspartate (●), 50 mM D-glutamate (○), and 25 mM NMDA (△).The final concentration of the holo-subunit of the enzyme (E_t) was 32.2 nM. The lines drawn in the figures are made on the basis of Eq. 5 using the corresponding best-fit values of the four kinetic parameters listed in Table 4.

Table 4. **Apparent kinetic parameters of DDO for O_2 obtained using D-aspartate (25 mM), D-glutamate (50 mM), and NMDA (25 mM).** The data was fitted to Equation 5. The best-fit values for the parameters are listed with the standard deviation.

Substrate	K_{mO2}^{app} (μM)	k_{cat}^{app} (s^{-1})	$k_{cat}^{app}/K_{mO2}^{app}$ ($M^{-1}\,s^{-1}$)
D-Aspartate	613 ± 424	172 ± 65	2.81×10^5
D-Glutamate	547 ± 496	30.0 ± 14	5.48×10^4
NMDA	$(2.01 \pm 1.37) \times 10^3$	635 ± 325	3.16×10^5

catalyzes similar oxidative deamination of D-amino acids with non-anionic side-chain groups and plays important roles in the metabolism of D-serine, a gliotransmitter, in the mammalian brain (*e.g. 1*, *30*). Purification of mammalian DDO has succeeded only from bovine kidney prior to this study. The purified porcine DDO is a homotetramer, whereas bovine DDO is a monomeric enzyme (*16*). The porcine DDO contained noncovalently bound FAD as a coenzyme. Unlike DDO purified from bovine kidney cortex (*16*), the porcine enzyme contained no 6-hydroxy-FAD. The N-terminal amino acid of the native porcine DDO was somewhat modified, whereas that of the recombinant DDO was not modified. However, the presence and absence of the modification of the N-terminal residue was not important for activity. Multiple forms of DDO mRNA have been isolated from human brain (*19*) and mouse tissues (*14*). However, a single active peak of DDO always appeared during all of the chromatography stages used for the purification of DDO from porcine kidney, suggesting that only one active form of DDO protein is expressed in porcine kidney.

We isolated and sequenced the complete cDNA coding for the porcine DDO for the first time, and overexpressed the recombinant DDO in *E. coli* cells. We did not find any significant difference in catalytic properties between the native and recombinant DDOs.

DDO from bovine kidney showed substrate activation at high D-aspartate concentrations (*23–25*), resulting in a downward curved Lineweaver-Burk plot (the $1/v$ versus $1/[S]$ plot). Porcine DDO showed similar substrate activation for D-aspartate. In addition to D-aspartate, substrate activation of porcine DDO was also found for D-glutamate. Interestingly, porcine DDO was subject to substrate inhibition at high NMDA concentrations.

Both activation and inhibition by high concentrations of D-amino acid substrates can be explained by the

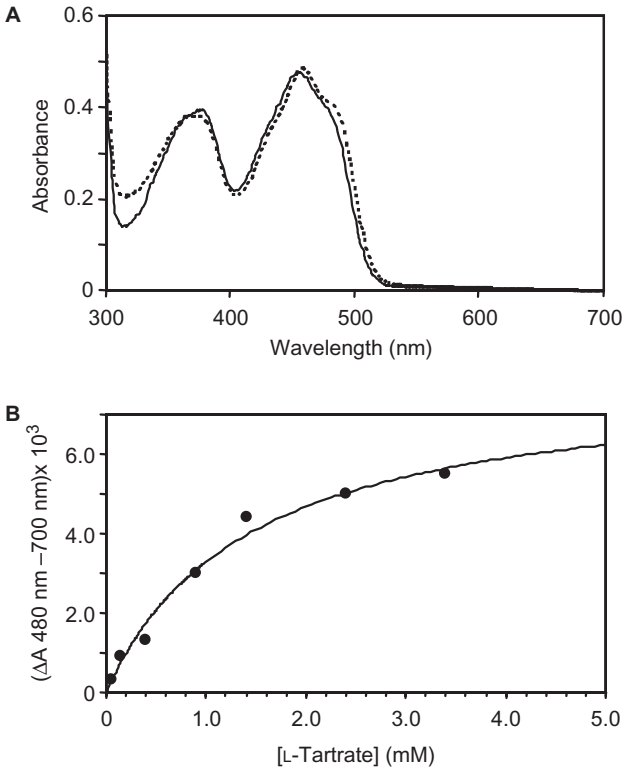

Fig. 9. **Titration of porcine DDO with L-tartrate.** Aliquots of L-tartrate stock solution were added to recombinant porcine DDO (10 μM) in 50 mM sodium phosphate, pH 6.75, at 37°C, to give the final concentrations indicated. (A) Absorption spectra of DDO without (–) and with (. . .) 10 mM L-tartrate. (B) Plot of the difference in absorption at 480 nm and 700 nm versus the total concentration of L-tartrate. The line drawn in the figure was made on the basis of Eq. 1 using the best-fit value of K_d listed in Table 5 and ΔA_∞ value of 8.0×10^{-3}.

reaction model shown in Fig. 1. There are two important points in this model, as Hamilton has pointed out (*25*). The first point is that the complex between the reduced form of enzyme and the imino-acid product (E_r–P) releases the product (P) more rapidly than the oxidation of the E_r–P complex by O_2. Due to this rapid release of product, substantial levels of free reduced form DDO (E_r) are produced under steady-state conditions. In the case of the D-amino acid oxidase reaction, it is supposed that the E_r–P complex is rapidly oxidized to the oxidized form enzyme–product complex (E_o–P) without the release of the product from the E_r–P complex (*26*, *37*); the bound product facilitates the oxidation of the reduced FAD coenzyme by O_2 (*26*). In fact, probably due to the lack of the production of free reduced enzyme, neither substrate activation nor substrate inhibition has been observed for D-amino acid oxidase. The second point is that the free reduced form of DDO (E_r) catalyzes the reaction as follows: (1) binding of D-amino acid substrate (S) to form the E_r–S complex, (2) oxidation of the E_r–S complex by O_2 to produce the E_o–S complex and hydrogen peroxide, (3) dehydrogenation of the substrate in the E_o–S complex to produce the E_r–P complex, and finally (4) the release of the product from the E_r–P complex, and regeneration of the catalyst E_r.

Table 5. **The dissociation constant of porcine DDO for dicarboxylates determined at 37°C and pH 6.75.**

Dicarboxylate	K_d (mM)
meso-Tartrate	0.118 ± 0.023
L-Tartrate	1.44 ± 0.09
D-Tartrate	20.0 ± 0.1
Malonate	2.61 ± 0.12

If the oxidation rate of the free reduced form of the enzyme (E_r) by O_2 is higher than that of the E_r–S complex by O_2, then substrate inhibition will appear at higher concentrations of substrate, as observed for NMDA (Fig. 7I). If the oxidation rate of the E_r–S complex is higher than that of free E_r, then substrate activation will appear at higher substrate concentrations, as observed for D-aspartate and D-glutamate (Fig. 7C, D, G, and H). If there is no partition between the substrate binding to E_r and the oxidation of E_r (either $k_6 = 0$ or $k_8 = 0$ in Fig. 1), then Eq. 2 is transformed to a Michaelian type equation and no substrate activation/inhibition occurs.

Recently, engineering the substrate specificity of D-amino acid oxidase to accept dicarboxylic D-amino acids as substrates has been reported (*36*, *38*). However, substrate activation/inhibition has never been reported for these engineered D-amino acid oxidases. Although models of the active site structures of mouse and bovine DDOs have been built using the three-dimensional structure of D-amino acid oxidase and the homology in the amino acid sequences (*22*, *36*), the three-dimensional structure of DDO has never been solved hitherto. Interestingly, bacterial L-aspartate oxidase, which has no sequence homology with DDO, also exhibits prominent substrate activation at L-aspartate concentrations above 1.0 mM (*39*).

Apparent k_{cat} and K_m values for DDO from various sources have been determined using a linear portion of the Lineweaver-Burk plots obtained at higher concentrations of D-amino acid substrates. In the present model of DDO reaction, the corresponding values of k_{cat} and K_m can be calculated according to Eqs E20 and E21 (see Appendix) using the kinetic parameters listed in Table 2. The results are summarized in Table 6 together with the apparent k_{cat} and K_m values reported for bovine and human DDOs. The apparent k_{cat}/K_m values of porcine and bovine DDOs for D-aspartate are smaller than those for NMDA by 3.8- and 3.4-fold, respectively, whereas the apparent k_{cat}/K_m value of human DDO for D-aspartate is 3.5-fold larger than that for NMDA. All of the apparent k_{cat}/K_m values of porcine, bovine, and human DDOs for D-aspartate are in the order of $1 \times 10^4\,M^{-1}\,s^{-1}$. These results suggest that the catalytic efficiency and the substrate preference of porcine DDO at higher substrate concentrations are similar to those of bovine and human DDO.

As the concentration of D-aspartate at physiological conditions is in the range of 0–3 mM (*1*, *3*, *5*), the kinetic properties of DDO at lower concentrations of D-aspartate are important. As explained in the Appendix, the initial portion of the v versus [S] curve is characterized by the apparent k_{cat} and K_m values defined by Eqs E16 and E17. These values are summarized in Table 7. At lower

Table 6. **Comparison of apparent kinetic parameters of mammalian DDO for D-aspartate, D-glutamate, and NMDA at high substrate concentrations.**

Substrate	K_m^{app} (mM)	k_{cat}^{app} (s^{-1})	k_{cat}^{app}/K_m^{app} ($M^{-1}s^{-1}$)
Porcine[a]			
D-Aspartate	2.52	37.5	1.49×10^4
D-Glutamate	66.9	9.36	1.40×10^2
NMDA	0.853	45.1	5.29×10^4
Bovine[b]			
D-Aspartate	3.7	22.5	6.1×10^3
D-Glutamate	5.6	1.19	2.1×10^2
NMDA	1.5	30.9	2.1×10^4
Human[c]			
D-Aspartate	2.7	52.5	1.9×10^4
D-Glutamate	N.D.[d]	N.D.[d]	N.D.[d]
NMDA	6.8	37.7	5.5×10^3

[a]Except for NMDA, these values are calculated by $k_{cat} = 1/A_5$ (Eq. E20) and $K_m = A_4/A_5$ (Eq. E21), and the values of A_4 and A_5 in Table 2. Those for NMDA are the same values as listed in Table 7. [b]Taken from reference 23 (50 mM sodium phosphate, pH 7.4, 25°C). [c]Taken from reference 19 (50 mM sodium pyrophosphate, pH 8.3, 25°C). [d]N.D., not determined.

Table 7. **Apparent kinetic parameters of DDO for dicarboxylic D-amino acids at low substrate concentrations.** The apparent kinetic parameters are calculated according to Equations E16 and E17 (see Appendix) using the values of A_1, A_3, and A_4 in Table 2.

Substrate	K_m^L (μM)	k_{cat}^L (s^{-1})	k_{cat}^L/K_m^L ($M^{-1}s^{-1}$)
D-Aspartate	13.3	2.63	1.98×10^5
D-Glutamate	577	3.19	5.53×10^3
NMDA	853	45.1	5.29×10^4

concentrations of D-amino acid substrates, the apparent k_{cat}/K_m value of porcine DDO for D-aspartate is 3.7-fold larger than that for NMDA, indicating that the relative catalytic efficiency is reversed by low or high concentrations of substrate.

In conclusion, we have revealed for the first time the kinetic and structural properties of porcine DDO. Substrate activation/inhibition of porcine DDO was successfully analyzed by a reaction model where the oxidase shows different catalytic properties depending on the redox states of FAD. To further elucidate the molecular mechanism of substrate activation/inhibition of the oxidase, crystallographic and transient-state kinetic studies are necessary. In addition, the crystal structure of FAD-bound L-aspartate oxidase from *E. coli* has been solved (*40*). Considering the information accumulated for DDO and the related enzymes together, the redox-dependent interaction of DDO with substrate and imino-acid product seems to play key roles in the substrate activation/inhibition of DDO.

Supplementary data are available at JB online.

The present study was supported by a Grant-in Aid for Scientific Research (C) (NO. 18590528) (to T. I., and H. T.) from the Ministry of Education, Culture, Sports, Sciences, and Technology of Japan, and Grant-in Aid (Heisei era 18) from Shiga University of Medical Science. The nucleotide sequence data reported in this paper will appear in the DDBJ, EMBL and GenBank nucleotide sequence databases with accession number AB271762.

REFERENCES

1. Hashimoto, A. and Oka, T. (1997) Free D-aspartate and D-serine in the mammalian brain and periphery. *Progr. Neurobiol.* **52**, 325–353
2. Schell, M.J., Cooper, O.B., and Snyder, S.H. (1997) D-aspartate localizations imply neuronal and neuroendocrine roles. *Proc. Natl. Acad. Sci. USA* **94**, 2013–2018
3. Lee, J.-A., Homma, H., Tashiro, K., Iwatsubo, T., and Imai, K. (1999) D-Aspartate localization in the rat pituitary gland and retina. *Brain Res.* **838**, 193–199
4. Wolosker, H., D'Aniello, A., and Snyder, S.H. (2000) D-Aspartate disposition in neuronal and endocrine tissues: ontogeny, biosynthesis and release. *Neuroscience* **100**, 183–189
5. D'Aniello, A., Di Fiore, M.M., Fisher, G.H., Milone, A., Seleni, A., D'Aniello, S., Perna, A.F., and Ingrosso, D. (2000) Occurrence of D-aspartic acid and *N*-methyl-D-aspartic acid in rat neuroendocrine tissues and their role in the modulation of luteinizing hormone and growth hormone release. *FASEB J.* **14**, 699–714
6. Wang, H., Wolosker, H., Morris, J.F., Pevsner, J., Snyder, S.H., and Selkoe, D.J. (2002) Naturally occurring free D-aspartate is a nuclear component of cells in the mammalian hypothalamo-neurohypophyseal system. *Neuroscience* **109**, 1–4
7. Homma, H. (2007) Biochemistry of D-aspartate in mammalian cells. *Amino Acids* **32**, 3–11
8. Takigawa, Y., Homma, H., Lee, J.-A., Fukushima, T., Santa, T., Iwatsubo, T., and Imai, K. (1998) D-Aspartate uptake into cultured rat pinealocytes and the concomitant effect on L-asparate levels and melatonin secretion. *Biochem. Biophys. Res. Commun.* **248**, 641–647
9. Long, Z., Lee, J.-A., Okamoto, T., Nimura, N., Imai, K., and Homma, H. (2000) D-Aspartate in a prolactin-secreting clonal strain of rat pituitary tumor cells (GH_3). *Biochem. Biophys. Res. Commun.* **276**, 1143–1147
10. D'Aniello, G., Tolino, A., D'Aniello, A., Errico, F., Fisher, G.H., and Di Fiore, M.M. (2000) The role of D-aspartic acid and *N*-methyl-D-aspartic acid in the regulation of prolactin release. *Endocrinology* **141**, 3862–3870
11. Wang, H., Wolosker, H., Pevsner, J., Synder, S.H., and Selkoe, D.J. (2000) Regulation of rat magnocellular neurosecretory system by D-aspartate: evidence for biological role(s) of a naturally occurring free D-amino acid in mammals. *J. Endocrinol.* **167**, 247–252
12. Nakatsuka, S., Hayashi, M., Muroyama, A., Otsuka, M., Kozaki, S., Yamada, H., and Moriyama, Y. (2001) D-Aspartate is stored in secretary granules and released through a Ca^{2+}-dependent pathway in a subset of rat pheochromocytoma PC12 cells. *J. Biol. Chem.* **276**, 26589–26596
13. Huang, A.S., Beigneux, A., Weil, Z.M., Kim, P.M., Molliver, M.E., Blackshaw, S., Nelson, R.J., Young, S.G., and Snyder, S.H. (2006) D-Aspartate regulates melanocortin formation and function: behavioral alterations in D-aspartate oxidase-deficient mice. *J. Neurosci.* **26**, 2814–2819
14. Errico, F., Pirro, M.T., Affuso, A., Spinelli, P., De Felice, M., D'Aniello, A., and Di Lauro, R. (2006) A physiological mechanism to regulate D-aspartic acid and NMDA levels in mammals reveled by D-aspartate oxidase deficient mice. *Gene* **374**, 50–57
15. Weil, Z.M., Huang, A.S., Beigneux, A., Kim, P.M., Molliver, M.E., Blackshaw, S., Young, S.G., Nelson, R.J., and Snyder, S.H. (2006) Behavioural alterations in male mice lacking the gene for D-aspartate oxidase. *Behaviour. Brain Res.* **171**, 295–302
16. Negri, A., Massey, V., and Williams, Jr., C.H. (1987) D-Aspartate oxidase from beef kidney. Purification and properties. *J. Biol. Chem.* **262**, 10026–10034

17. De Marco, C. and Crifò, C. (1967) D-Aspartate oxidase from pig kidney. 3. Competitive inhibition by dicarboxylic hydroxyacids. *Enzymologia* **33**, 325–330
18. Jaroszewicz, L. (1975) D-Aspartate oxidase in the thyroid gland. *Enzyme* **20**, 80–89
19. Setoyama, C. and Miura, R. (1997) Structural and functional characterization of the human brain D-aspartate oxidase. *J. Biochem.* **121**, 798–803
20. Simonic, T., Duga, S., Negri, A., Tedeschi, G., Malcovati, M., Tenchini, M.L., and Ronchi, S. (1997) cDNA cloning and expression of the flavoprotein D-aspartate oxidase from bovine kidney cortex. *Biochem. J.* **322**, 729–735
21. Negri, A., Tedeschi, G., Ceciliani, F., and Ronchi, S. (1999) Purification of beef kidney D-aspartate oxidase overexpressed in *Escherichia coli* and characterization of its redox potentials and oxidative activity towards agonists and antagonists of excitatory amino acid receptors. *Biochim. Biophys. Acta* **1431**, 212–222
22. Katane, M., Furuchi, T., Sekine, M., and Homma, H. (2007) Molecular cloning of a cDNA encoding mouse D-aspartate oxidase and functional characterization of its recombinant proteins by site-directed mutagenesis. *Amino Acids* **32**, 69–78
23. Negri, A., Massey, V., Williams, Jr., C.H. and Schopfer, L.M. (1988) The kinetic mechanism of beef kidney D-aspartate oxidase. *J. Biol. Chem.* **263**, 13557–13563
24. Nasu, S., Wicks, F.D., and Gholson, R.K. (1982) The mammalian enzyme which replaces B protein of *E. coli* quinolinate synthetase is D-aspartate oxidase. *Biochim. Biophys. Acta* **704**, 240–252
25. Hamilton, G.A. (1985) Peroxisomal oxidases and suggestions for the mechanism of action of insulin and other hormones in *Advances in Enzymology* (Meister, A., ed.) Vol. 57, pp. 85–178, John Wiley & Sons, New York
26. Mizutani, H., Miyahara, I., Hirotsu, K., Nishina, Y., Shiga, K., Setoyama, C., and Miura, R. (2000) Three-dimensional structure of the purple intermediate of porcine kidney D-amino acid oxidase. Optimization of the oxidative half-reaction through alignment of the product with reduced flavin. *J. Biochem.* **128**, 73–81
27. Harris, C.M., Pollegioni, L., and Ghisla, S. (2001) pH and kinetic isotope effects in D-amino acid oxidase catalysis. Evidence for a concerted mechanism in substrate dehydrogenation via hydride transfer. *Eur. J. Biochem.* **268**, 5504–5520
28. Yamada, R., Nagasaki, H., Wakabayashi, Y., and Iwashima, A. (1988) Presence of D-aspartate oxidase in rat liver and mouse tissues. *Biochim. Biophys. Acta* **965**, 202–205
29. Nakajima, H., Ishida, T., Tanaka, H., and Horiike, K. (2002) Accurate measurement of near-micromolar oxygen concentrations in aqueous solutions based on enzymatic extradiol cleavage of 4-chlorocatechol: application to improved low-oxygen experimental systems and quantitative assessment of back diffusion of oxygen from the atmosphere. *J. Biochem.* **131**, 523–531
30. Tanaka, H., Yamamoto, A., Ishida, T., and Horiike, K. (2007) Simultaneous measurement of D-serine dehydratase and D-amino acid oxidase activities by the detection of 2-oxo-acid formation with reverse-phase HPLC. *Anal. Biochem.* doi:10.1016/j.ab.2006.12.025
31. Whitby, L.G. (1953) A new method for preparing flavin-adenine dinucleotide. *Biochem. J.* **54**, 437–442
32. Laemmli, U.K. (1970) Cleavage of structural proteins during the assembly of the head of bacteriophage T4. *Nature* **227**, 680–685
33. Yu, L., Ishida, T., Ozawa, K., Akutsu, H., and Horiike, K. (2001) Purification and characterization of homo- and heterodimeric acetate kinases from the sulfate-reducing bacterium *Desulfovibrio vulgaris*. *J. Biochem.* **129**, 411–421
34. Kobayashi, T., Ishida, T., Horiike, K., Takahara, Y., Numao, N., Nakazawa, A., Nakazawa, T., and Nozaki, M. (1995) Overexpression of *Pseudomonas putida* catechol 2,3-dioxygenase with high specific activity by genetically engineered *Escherichia coli*. *J. Biochem.* **117**, 614–622
35. Gould, S.J., Keller, G.-A., Hosken, N., Wilkinson, J., and Subramani, S. (1989) A conserved tripeptide sorts proteins to peroxisomes. *J. Cell. Biol.* **108**, 1657–1664
36. Sacchi, S., Lorenzi, S., Molla, G., Pilone, M.S., Rossetti, C., and Pollegioni, L. (2002) Engineering the substrate specificity of D-amino-acid oxidase. *J. Biol. Chem.* **277**, 27510–27516
37. Umhau, S., Pollegioni, L., Molla, G., Diederichs, K., Welte, W., Pilone, M.S., and Ghisla, S. (2000) The x-ray structure of D-amino acid oxidase at very high resolution identifies the chemical mechanism of flavin-dependent substrate dehydrogenation. *Proc. Natl. Acad. Sci. USA* **97**, 12463–12468
38. Setoyama, C., Nishina, Y., Mizutani, H., Miyahara, I., Hirotsu, K., Kamiya, N., Shiga, K., and Miura, R. (2006) Engineering the substrate specificity of porcine kidney D-amino acid oxidase by mutagenesis of the "active-site lid". *J. Biochem.* **139**, 873–879
39. Nasu, S., Wicks, F.D., and Gholson, R.K. (1982) L-Aspartate oxidase, a newly discovered enzyme of *Escherichia coli*, is the B protein of quinolinate synthetase. *J. Biol. Chem.* **257**, 626–632
40. Bossi, R.T., Negri, A., Tedeschi, G., and Mattevi, A. (2002) Structure of FAD-bound L-aspartate oxidase: Insight into substrate specificity and catalysis. *Biochemistry* **41**, 3018–3024

APPENDIX

The reaction mechanism proposed in the present study for porcine D-aspartate oxidase catalysis of oxidative deamination of D-aspartate (Fig. 1) prescribes the following rate equation under steady-state conditions.

$$\frac{v}{E_t} = \frac{a_1[S] + a_2[S]^2}{a_3 + a_4[S] + a_5[S]^2} \tag{E1}$$

where v, E_t, and [S] denote the initial velocity, the total concentration of the enzyme active site, and the concentration of D-amino acid substrates, respectively. The parameters (a_1–a_5) in Eq. E1 are given by

$$a_1 = k_1k_2k_5k_8(k_3[O_2] + k_4)(k_{-6} + k_7[O_2])[O_2] \tag{E2}$$

$$a_2 = k_1k_2k_5k_6k_7(k_3[O_2] + k_4)[O_2] \tag{E3}$$

$$a_3 = k_5k_8(k_{-6} + k_7[O_2])\{k_{-1}k_{-2} + k_{-1}k_4 + k_2k_4 + (k_{-1} + k_2)k_3[O_2]\}[O_2] \tag{E4}$$

$$a_4 = k_5k_6k_7\{(k_{-2} + k_4)k_{-1} + (k_{-1} + k_2)k_3[O_2]\}[O_2] + k_1(k_{-6} + k_7[O_2])\{k_2k_5(k_4 + k_8[O_2]) + k_5k_8(k_{-2} + k_4)[O_2] + k_3k_8(k_2 + k_5)[O_2]^2\} \tag{E5}$$

$$a_5 = k_1k_2k_4k_5k_6 + k_1k_6k_7\{k_5(k_2 + k_{-2} + k_4) + k_3(k_2 + k_5)[O_2]\}[O_2] \tag{E6}$$

If $k_3 = 0$, then the model becomes the same as Hamilton's model (*25*). If $k_6 = 0$, then the model becomes the same one proposed for D-amino acid oxidase catalysis (*26*, *27*), and Eq. E1 becomes an ordinary equation of Michaelis–Menten type.

Equation E1 can be expressed in the following form after some algebra.

$$\frac{[S]}{(v/E_t)} = \frac{A_3 + A_4[S] + A_5[S]^2}{A_1 + [S]} \quad \text{(E7)}$$

where A_i is defined by a_i/a_2 ($i = 1$, 3, 4, and 5), respectively. This equation shows that the [S]/v versus [S] plot of kinetic data is characterized by four kinetic parameters of A_1, A_3, A_4, and A_5. Using Eqs E2–E6, the relations between the A_i and the elementary rate constants (Fig. 1) are given as follows:

$$A_1 = k_8[O_2]\left(\frac{1}{k_6} + K_R \cdot \frac{1}{k_7[O_2]}\right) \quad \text{(E8)}$$

$$A_3 = A_1\left[\frac{1}{k_1} + K_O \cdot \frac{1}{k_2} + K_O \frac{1}{(k_3[O_2] + k_4)}\right] \quad \text{(E9)}$$

$$A_4 = \left(\frac{1}{k_3[O_2] + k_4}\right)\left[K_O\left(K_2 + \frac{k_4}{k_2} + \frac{k_3[O_2]}{k_2}\right) + \frac{k_3[O_2]}{k_1} + A_1\left(1 + K_2 + \frac{k_4}{k_2} + \frac{k_3[O_2]}{k_2} + \frac{k_3[O_2]}{k_5} + \frac{k_4}{k_8[O_2]}\right)\right] \quad \text{(E10)}$$

$$A_5 = \left(\frac{1}{k_3[O_2] + k_4}\right)\left(1 + K_2 + \frac{k_4}{k_2} + \frac{k_3[O_2]}{k_2} + \frac{k_3[O_2]}{k_5} + \frac{k_4}{k_7[O_2]}\right) \quad \text{(E11)}$$

where the equilibrium constants of K_R, K_O, and K_2 are given as follows:

$$K_R = \frac{k_{-6}}{k_6} \quad \text{(E12)}$$

$$K_O = \frac{k_{-1}}{k_1} \quad \text{(E13)}$$

$$K_2 = \frac{k_{-2}}{k_2} \quad \text{(E14)}$$

Approximate Expressions—When the substrate concentration is sufficiently low so that [S] is much smaller than A_1 and A_4/A_5, then Eq. E7 approximates to the following Michaelis–Menten type equation.

$$\frac{v}{E_t} = \frac{k_{cat}^L[S]}{K_m^L + [S]} \quad \text{(E15)}$$

where k_{cat}^L and K_m^L are defined by the following equations.

$$k_{cat}^L = \frac{A_1}{A_4} \quad \text{(E16)}$$

$$K_m^L = \frac{A_3}{A_4} \quad \text{(E17)}$$

In this low concentration range of substrate, using Eqs E8 and E9 the apparent substrate specificity constant is given as follows:

$$\frac{k_{cat}^L}{K_m^L} = \frac{1}{[(1/k_1) + K_O \cdot (1/k_2) + K_O(1/(k_3[O_2] + k_4))]} \quad \text{(E18)}$$

On the other hand, when the substrate concentration is sufficiently high so that [S] is much larger than A_1 and A_3/A_4, then Eq. E7 approximates to the following Michaelis–Menten type equation.

$$\frac{v}{E_t} = \frac{k_{cat}^H[S]}{K_m^H + [S]} \quad \text{(E19)}$$

where k_{cat}^H and K_m^H are defined by the following equations.

$$k_{cat}^H = \frac{1}{A_5} \quad \text{(E20)}$$

$$K_m^H = \frac{A_4}{A_5} \quad \text{(E21)}$$

In this high concentration range of substrates, the apparent substrate specificity constant is given as follows:

$$\frac{k_{cat}^H}{K_m^H} = \frac{1}{A_4} \quad \text{(E22)}$$

Dependence of the Initial Velocity on O_2 Concentration—Using Eqs E7–E11 and taking the limit of the reaction conditions saturated with D-amino acid substrate, Eq. E7 approximates the following equation:

$$\frac{[O_2]}{(v/E_t)} = \frac{B_3 + B_4[O_2] + B_5[O_2]^2}{B_1 + [O_2]} \quad \text{(E23)}$$

where B_1, B_3, B_4, and B_5 are given as follows:

$$B_1 = \frac{k_4}{k_3} \quad \text{(E24)}$$

$$B_3 = \frac{k_4}{k_3 k_7} \quad \text{(E25)}$$

$$B_4 = \frac{1}{k_3}\left(1 + \frac{k_{-2}}{k_2} + \frac{k_4}{k_2}\right) \quad \text{(E26)}$$

$$B_5 = \left(\frac{1}{k_2} + \frac{1}{k_5}\right) \quad \text{(E27)}$$

When the O_2 concentration is sufficiently low so that [O_2] is much smaller than B_1 and B_4/B_5, then Eq. E23 approximates to the following Michaelis–Menten type equation.

$$\frac{v}{E_t} = \frac{k_{cat}^{app}[O_2]}{K_{mO2}^{app} + [O_2]} \quad \text{(E28)}$$

where k_{cat}^{app} and K_{mO2}^{app} are defined by the following equations.

$$k_{cat}^{app} = \frac{B_1}{B_4} \quad \text{(E29)}$$

$$K_{mO2}^{app} = \frac{B_3}{B_4} \quad \text{(E30)}$$

In this low concentration range of substrate, the apparent substrate specificity constant is given as follows:

$$\frac{k_{cat}^{app}}{K_{mO2}^{app}} = k_7 \quad \text{(E31)}$$